Hydrogel-forming microarray patches with cyclodextrin drug reservoirs for long-acting delivery of poorly soluble cabotegravir sodium for HIV Pre-Exposure Prophylaxis

Fabiana Volpe-Zanutto [a,b], Lalitkumar K. Vora [a], Ismaiel A. Tekko [a,c], Peter E. McKenna [a], Andi Dian Permana [a,d], Akmal H. Sabri [a], Qonita K. Anjani [a], Helen O. McCarthy [a], Alejandro J. Paredes [a], Ryan F. Donnelly [a,*]

[a] *School of Pharmacy, Queen's University Belfast, 97 Lisburn Road, Belfast BT9 7BL, UK*
[b] *Faculty of Pharmaceutical Sciences, R. Cândido Portinari, 200 - Cidade Universitária, Campinas - SP, 13083-871, University of Campinas, Brazil*
[c] *Faculty of Pharmacy, Aleppo University, Syria*
[d] *Department of Pharmaceutics, Faculty of Pharmacy, Hasanuddin University, Makassar, Indonesia*

ARTICLE INFO

ABSTRACT

Hydrogel-forming microarray patches (HF-MAPs) offer minimally invasive, pain-free and prolonged drug delivery. These devices are designed to be self-administered and self-disabling, avoiding contaminated sharps waste generation. Cabotegravir sodium (CAB-Na) is a poorly soluble anti- human immunodeficiency virus (HIV) drug for the treatment and pre-exposure prophylaxis of HIV infection that lends itself to depot formation following intradermal delivery but presents significant challenges when delivered *via* HF-MAPs, whose nature is aqueous. Herein, we have investigated, for the first time, the use of hydroxypropyl-β-cyclodextrin (HP-β-CD) to enhance the solubility of CAB-Na, and its effect on intradermal delivery *via* HF-MAPs. Accordingly, tablet reservoirs containing CAB-Na and HP-β-CD were formulated. These novel reservoirs were combined with two different HF-MAP formulations (MAP1 (Gantrez S97® + poly (ethylene glycol) 10,000 + Na_2CO_3) and MAP2 (poly (vinyl pyrrolidone) 58 kDa + poly (vinyl alcohol) 85–120 kDa + citric acid)) to form fully integrated MAP devices which were tested in both *ex vivo* and *in vivo* settings. *Ex vivo* skin deposition results for MAP1 and MAP2 showed that 141 ± 40 µg and 342 ± 34 µg of CAB-Na was deposited into $0.5 \ cm^2$ of excised neonatal porcine skin after 24 h, respectively. Based on these findings, the *in vivo* pharmacokinetics of MAP2 were investigated over 28 days using a Sprague-Dawley rat model. After 24 h patch application, MAP2 demonstrated an extended drug release profile and an observed C_{max} of 53.4 ± 10.16 µg/mL, superior to that of an FDA-approved CAB-nanosuspension administered *via* intramuscular application (C_{max} of 43.6 ± 5.3 µg/mL). Consequently, this tablet integrated MAP device is considered to be a viable option for the intradermal delivery of hydrophobic anti-HIV drugs.

1. Introduction

The first cases of acquired immunodeficiency syndrome (AIDS), an illness caused by human immunodeficiency virus (HIV), were reported in 1981 [1]. Since then, HIV has claimed approximately 36 million lives and it is projected that at the end of 2020 that there were 37.7 million people living with HIV, 25.4 million of which are concentrated in Sub-Saharan Africa, yet only 27.5 million people are receiving antiretroviral therapy (ART) [2,3] Currently, there are an estimated 1.5 million new HIV infections each year and, in 2020 alone, approximately

680,000 deaths were attributed to HIV-related illnesses [4,5]. Current ART strategies can be costly, which limits the accessibility of ART for those living in lower- and middle-income areas within the region of Sub-Saharan Africa [6,7]. Furthermore, in this region, the availability of trained healthcare staff for application of parenteral treatment (who are required for ART in its current form) is low, which negatively impacts the rate of successful treatment. Pre-exposure prophylaxis (PrEP) is a highly effective pharmacological tool used for the purpose of HIV prevention among high-risk groups [6]. Effective use of PrEP has previously demonstrated a significant reduction in new HIV infections among high-

---

risk individuals from 86% to 44% [8,10].

Cabotegravir (CAB) is one of the most promising ART drugs available for PrEP, due to its high effectiveness and reduced occurrence of collateral side effects when compared to other compounds [8–12]. CAB is an analogue of dolutegravir (DOL) and acts as an integrase strand transfer inhibitor [10]. Aiming to develop a parentally administered, long-acting (LA) PrEP for HIV, CAB-Nanosuspension (CAB-LA) was formulated for intramuscular administration, being the first long-acting injection approved for HIV PrEP. In 2021, the US FDA (Food and Drug Administration) authorised the first long-acting treatment of HIV infection in adults containing the combination of CAB-Nanosuspension (CAB LA) and rilpivirine (RPV LA). [13].

CAB LA overcomes the drawbacks related with oral dosing of CAB, extending its half-life by 25-fold (25–52 days in humans). CAB LA can be administered for PrEP in negative-HIV individuals with high risk of infection *via* intramuscular injection (IM) monthly (400 mg) or bimonthly (800 mg), thus, reducing dosing frequency and improving patient adherence [8,14]. However, parenteral administration requires the use of a hypodermic needle, which many individuals find unacceptable due to needle phobia [15]. Moreover, parenterally-administered products generate clinical sharps waste, a significant issue, especially in the case of HIV treatment. This presents a substantial HIV transmission risk to both patients and healthcare workers, with those in low and middle income regions having higher incidences of unsafe injection practices [16–18]. Other issues that still need to be addressed include the cost of CAB-LA manufacturing, which is both energy and labour-intensive, and the fact that transport in low- and middle- income regions is often challenging and, as a result, many people simply cannot access the treatment that they need. Whilst CAB-LA greatly improves the experience of a patient receiving treatment, it requires administration by trained healthcare staff. Thus, it faces obstacles to widespread use in low-resource countries with insufficient healthcare workers [5,16,19–22]. Therefore, the development of alternative LA formulations that are inexpensive to manufacture, demonstrate reduced side effect incidence, and that can be self-administered is an exciting concept to be explored.

A microarray patch (MAPs) is composed of an array of micron-sized needles arranged on a flat baseplate. Upon application, microneedles (MNs) pierce the *stratum corneum,* the outermost layer of the skin, and deliver therapeutics intradermally without eliciting pain or bleeding [23,24]. Significantly, MAPs are designed to be self-administered *i.e.,* trained healthcare staff are not required for their use. Furthermore, certain MAP types, namely hydrogel-forming and dissolving MAPs, are self-disabling in nature, meaning that they are not capable of re-insertion in the skin after use, thus effectively eliminating the risk of infection transmission [24–26]. Hydrogel-forming MAPs (HF-MAPs) are a type of MAP made from a cross-linked polymer matrix that absorbs interstitial fluid from the skin upon application to form a hydrogel *in situ* [25,55]. In contrast to other MAP types, where the drug is loaded into or onto individual MNs, hydrogel-forming MAPs have a separately-formulated drug reservoir that is connected to the back of the MN array. Upon sufficient swelling of the array, this drug reservoir dissolves, releasing drug into the inserted hydrogel, from which it is delivered intradermally in a rate-controlled manner [27]. Crucially, this two-part design facilitates enhanced drug loading and further expands the range of deliverable molecules to include not only potent low-dose molecules, but also those that require high doses. Although intrinsically well-suited for the delivery of hydrophilic drug molecules, hydrophobic compounds may also be successfully delivered using this platform, when combined with a suitable solubility-enhancing technique [28].

In this work, the aqueous solubility of CAB-Na was enhanced by complexing the drug with cyclodextrin (CD) molecules. CDs are cyclic oligosaccharides that possess a truncated cone structure and are classified as α, β, or γ types, which contain six, seven, and eight glucose units, respectively. Importantly, they have a hydrophobic inner cavity which is surrounded by a hydrophilic outer surface [29]. This structure allows them to interact with and house hydrophobic compounds in their inner cavity, whilst simultaneously solubilising themselves and the drug in an aqueous environment [30]. In the present study, CAB-Na was combined with hydroxypropyl-β-cyclodextrin to formulate the suitable tablet reservoir that dissolved rapidly and completely when situated atop a swollen HF-MAP. Intradermal delivery of this anti-HIV therapeutic was achieved over 24 h in rats *in vivo* and drug pharmacokinetics were studied over the following 28 days, revealing that the formulated HF-MAP device had a LA delivery profile. The work outlined within highlights, for the first time, the potential of this technology to overcome many issues commonly faced by patients who require HIV PrEP treatment, particularly in low-resource settings.

2. Material and methods

2.1. Materials

Cabotegravir sodium (CAB-Na) and cabotegravir long-acting (CAB LA) vials for intramuscular injection (CAB LA, 400 mg/2 mL) were provided by ViiV Healthcare (Brentford, UK). Polyvinylalcohol (PVA) molecular weight (m/w) of 85–120 kDa, 87%–89% hydrolysed, polyethyleneglycol (PEG) 10,000, Na_2CO_3 (sodium carbonate), acetonitrile (ACN) (HPLC grade), trifluoracetic acid, heparin, isoflurane, formic acid, citric acid, and phosphate buffered saline (PBS, pH 7.4) tablets were purchased from Sigma-Aldrich (Dorset, U.K). Gantrez® S-97 (copolymer of methylvinylether and maleic acid 1500 kDa (m/w)), polyvinylpyrrolidone (PVP) K29–32 (58 kDa m/w) and 2-hydroxypropyl-β-cyclodextrin (HP-β-CD) Cavitron™ W7HP7 Pharma were gifted from Ashland Inc. (Kidderminster, U.K.). All other materials and chemicals were of analytical reagent grade.

2.2. Fabrication of "Super-swelling" HF-MAPs

In this work, two HF-MAP formulations were studied. The first to be tested was a "Super swelling" [31] formulation which was composed of copolymer of methylvinylether and maleic acid (20% *w*/w), PEG 10,000 (7.5% w/w) and Na_2CO_3 (3% w/w) dispersed in deionized water [31]. Approximately 600 mg of the hydrogel was carefully dispensed into pre-formed silicone MAP moulds (MNs arranged in a 11 × 11 formation, 900 μm height, 300 μm needle width and 150 μm needle interspacing at the base) [32]. Filled moulds were centrifuged at 3500 RPM for 15 min and allowed to dry for 48 h at room temperature. Dried MAPs were then crosslinked for 24 h at 80 °C to induce ester-bonds between Gantrez® S-97 and PEG [31,57] (Table 1).

2.3. Fabrication of PVA/PVP HF-MAPs

The second HF-MAP formulation was composed of PVA (15% *w*/w), PVP (10% w/w), citric acid (1.5% w/w) dissolved in water [28]. In a similar fashion to the protocol for the fabrication of "Super-swelling" HF-MAPs, analogous MAP moulds were filled with the prepared aqueous blend, centrifuged at 3500 RPM for 15 min, dried at 25 °C for 48 h, and crosslinked according to the conditions outlined in Table 1.

Table 1
Hydrogel formulations and crosslinking conditions.

Formulation	Hydrogel Composition % (w/w)	Crosslinking Temperature °C	Crosslinking Time (h)
MAP1	Gantrez S97® (20%) + sodium carbonate (3%) + PEG 10,000 (7.5%)	80	24
MAP2	PVA (15%) + PVP (10%) Citric acid (1.5%)	130	1

2.4. Optical microscopy analysis and scanning electron microscopy (SEM)

The structure and morphology of the formulated MAPs was assessed by optical digital light microscopy (Leica EZ4D, Leica, Wetzlar, Germany) and scanning electron microscopy (SEM) (TM3030, Hitachi, Krefeld, Germany). For SEM analysis, MAPs were attached on an aluminum support with copper and carbon conductive tapes. The SEM images were taken by scanning with backscattered electrons at 15 kV [23].

2.5. Swelling studies of crosslinked MAPs

To investigate the swelling profiles of each MAP formulation, individual MAPs (0.5 cm^2) had their masses recorded in the dry state (m$_0$). They were then placed in an excess volume of water containing 5% *w/w* HP-β-CD and allowed to swell (*n* = 3). At pre-determined time points, the swollen MAPs were removed from the water, gently dabbed with filter paper to remove surface water and then re-weighed, with their masses recorded as m$_t$ [14]. Percentage swelling of each formulation was calculated using Eq. (1).

$$\%Swelling = \frac{(m_t - m_0)}{m_0} x100 \tag{1}$$

2.6. Rationalisation of CAB-Na/HP-β-CD

Phase-solubility analysis, as proposed by Higuchi and Connors, was employed to investigate the effect of HP-β-CD on the aqueous solubility of CAB-Na [33]. To characterise the solubility enhancement inferred by CD complexation and to optimise the formulation of drug/CD inclusion complexes, an excess of CAB-Na was put into aqueous solutions containing increasing concentrations of HP-β-CD (0, 5, 10 and 20% *w*/w). Samples were maintained at room temperature and gently agitated with magnetic stirrers until equilibrium was reached *i.e.,* until the amount of undissolved CAB-Na remained constant. At this point, the saturation solubility of CAB-Na in each of the CD concentrations tested was deduced by filtering samples through a 0.22 μm syringe filter to remove undissolved drug and then quantifying dissolved CAB-Na with HPLC-UV validated method (Section 2.17) [32,34].

2.7. Preparation of directly compressed tablets containing CAB-Na/HP-β-CD complexes

Solid state CAB-Na/HP-β-CD complexes were formed by lyophilisation of the aqueous solution containing the optimum concentration of HP-β-CD and CAB-Na [33,35]. Following lyophilisation using the Freeze Drier System (Virtis Advantage, SP Scientific Ltd., Warminster PA, USA), 250 mg of powdered inclusion complex was placed into a tablet die and compressed into tablets under manual hydraulic press (Specac Ltd., Kent, U.K.) with a compression force of 2 t for 20 s. The tablets produced contained 10 mg of CAB-Na, with a diameter and thickness of 13 mm and 1.4 mm, respectively.

2.8. Tablet characterisation

Characterisation of the formed directly compressed tablet reservoirs (*i.e.,* tablet diameter and thickness) was performed visually using a digital microscope (*n* = 6). Tablet dissolution time was measured by placing each tablet in 20 mL of deionized water with continuous stirring at 1200 RPM (*n* = 6).

2.9. Mechanical characterisation of HF-MAPs

Formulated HF-MAPs were characterised in terms of the percentage of height reduction, insertion efficiency, and insertion depth. To determine the height reduction, individual MNs was measured after compression for 30 s at 32 N onto an aluminum block utilising a TA.XT2 Texture Analyser (Stable Microsystems, Haslemere, UK) (force = 32 N) [36,37].

An optical coherence tomography (OCT) (EX1301 microscope, Michelson Diagnostics Ltd., Kent, UK) was employed to obtain cross-sectional images of HF-MAPs inserted into excised full-thickness porcine skin and the penetration depth of the MAPs in the skin (*n* = 6). The OCT configuration parameters were pre-established by Donnelly et al. [38]. The skin was removed from stillborn piglets, excised, and stored at −20 °C until use. Prior to use, the skin tissue was de-frosted and equilibrated in PBS (pH 7.4), at which point hair was carefully removed with help of manual disposable razor.

2.10. X-ray powder diffraction (XRD)

The XRD analyses were performed using a MiniFlex II powder X-Ray diffractometer (Rigaku Corporation, Tokyo, Japan), to evaluate the crystallinity of the drug, CD and drug/CD inclusion complex. Samples of CAB-Na, HP-β-CD and CAB-Na/HP-β-CD inclusion complex were individually placed into the rotating sample support. The analyses were performed in continuous mode within the range of 3–60°2θ (scanning rate of 2°/min) in triplicate. The analyses were carried using a current of 15 mA and a voltage of 30 kV. Furthermore, the diffractometer was equipped with a Ni filter, and Cu Kβ radiation was used to conduct the experiment [36].

2.11. Fourier transform infrared spectroscopy (FTIR)

The FTIR analyses of CAB-Na, HP-β-CD and the CAB-Na/HP-β-CD complex were performed using a FTIR spectrometer Cary 630 (Agilent, Santa Clara, California, USA) to identify the interactions that occur during inclusion complex formation. The IR experiment were scanned and recorded in between 4000 and 400 cm^{-1} at room temperature using attenuated total reflection (ATR) mode. Resolution was maintained at 4.0 cm^{-1} throughout all analyses and acquired spectra were the result of an average of 64 scans.

2.12. Identification of complex formation by NMR (methods)

NMR analyses of 1D: 1H and 2D: ROESY were performed using a spectrophotometer with a nuclear magnetic resonance of 11.7 Tesla (Varian® Inova). The samples were solublised in the deuterated dimethyl sulfoxide (DMSO-d_6) (Sigma-Aldrich® Co. Ltd. – Gillingham, Dorset, UK). Tetramethylsilane was applied as an internal standard.

2.13. Drug content

The drug content of directly compressed tablets (CAB-Na/HP-β-CD complex) was determined by dissolving each tablet in 10 mL of water (*n* = 6). The solution obtained was filtered using a syringe filter (0.22 μm), suitably diluted and analysed by validated HPLC-UV system (Section 2.17).

2.14. Skin drug deposition studies (ex vivo)

Ex vivo studies, which investigated the deposition of CAB-Na from the formulated HF-MAPs, were performed using full thickness neonatal porcine skin (treated and stored as explained in Section 2.9). The skin was affixed to the donor part of the Franz cell apparatus before the HF-MN array was inserted using manual pressure for 30 s. After insertion, 20 μL of PBS was aliquoted onto the baseplate of the array to promote reservoir adhesion and the formulated CAB-Na/HP-β-CD tablet was placed on top. To guarantee adequate insertion of the HF-MAP device throughout the study, a cylinder-shaped weight made of stainless-steel (12.0 g) was mounted on top of the CAB-Na/HP-β-CD tablet and the

Franz-cell apparatus was then sealed using Parafilm® M. To ensure sink conditions were maintained throughout, the receiver medium used was composed of HP-β-CD 5% *w*/w in deionized water (12 mL), degassed and pre-heated at 32 °C ± 1 °C. After 24 h, the apparatus was disassembled, the HF-MAP was removed, and the skin was separated from the donor compartment. Undeposited CAB-Na, which was visible on the side of the skin, was removed. Deposited drugs within the skin tissue were extracted according to the protocol in Section 2.15. Once again, samples (both from the skin and the donor compartment) were analysed with the HPLC-UV method outlined in Section 2.17.

2.15. Drug extraction from skin samples

Skin samples were cut from the MAP application site into tiny pieces using scissors and transferred to 2 mL centrifuge tubes having 500 μL of water +1 mL of acetonitrile. These samples were then homogenised for 15 min with stainless steel beads (5 mm diameter) using a TissueLyserLT (QIAGEN, U.K.) to extract the drug. The tissue samples were transferred to a 15 mL falcon tube, where 3.5 mL of acetonitrile: water (*v*/v) was added and left in ultrasonic bath for 1 h. Finally, samples were homogenised using vortex (1 min) and 100 μL of the supernatant was collected into 1.5 mL centrifuge tube containing 900 μL of acetonitrile, vortex 1 min, and centrifuged at 14,800 rpm for 10 min. The resulted supernatant was then transferred to 2 mL HPLC vials and the drug was quantified using HPLC-UV system.

2.16. Drug recovery from hydrogel-forming MAPs

Following completion of *ex vivo* skin deposition studies, the quantity of drug remaining in the swollen hydrogel MAPs was calculated by immersing the MAP in 5 mL acetonitrile and incubating samples at 37 °C ± 1 °C for 24 h to extract the drug. After incubation, the acetonitrile, into which CAB-Na had been extracted, was removed, and diluted appropriately with the same solvent. Samples were then vortexed for 2 min, centrifuged at 14,800 rpm for 10 min and subsequent analysed by HPLC-UV method.

2.17. HPLC-UV validation method (in vitro analysis)

Analysis of CAB-Na was carried out by using the reversed-phase HPLC (Agilent 1200® equipment, Agilent Technologies UK Ltd., UK) [32,34]. The UV detector was set at 257 nm, and the chromatographic separation was carried out using an Inertsil® ODS-3 C18 column (5 μm particle size and 150 mm length x 4.6 mm internal diameter) (GL Science Inc., Tokyo, Japan) maintained at 40 °C. Isocratic elution was employed with mobile phase which composed of ACN and 0.1% TFA (70:30 *v*/v). The injection volume of 40 μL and the flow rate was maintained at 0.8 mL/min. The data was obtained using an Agilent Chem-Station® Software (Version: B.02.01) and the analytical method validation was performed according to the corresponding International Council of Harmonisation (ICH) guidelines [32].

2.18. In vivo studies

An *in vivo* pharmacokinetic study of MAP2 combined with CAB-Na/ HP-β-CD directly compressed tablet reservoirs was conducted (Project Licence no. 2794). This *in vivo* experiment was reviewed and approved by the Queen's University Belfast Biological Services Unit Ethical Committee. Prior to study commencement, female rats (Sprague Dawley, 8–12 weeks of age) (205 ± 8 g) were acclimatised for 7 days and fasted overnight the day before study start. The rats were split into 2 groups (*n* = 6): Group 1 (control) – each rat was treated with an IM injection of CAB LA suspension 10 mg/rat, and Group 2 – each rat received four MAPs (MAP2 combined with CAB-Na/HP-β-CD) – Drug loading per tablet = 10 mg; total drug "dose" = 40 mg/rat. Approximately 24 h before MAP application, hair was removed from the backs of the rats in

Group 2 using Veet® depilatory cream (RB Healthcare, Ltd., Dansom Lane, Hull, UK). Applied MAPs were immobilised on the backs of each rat using adhesive foam and Tegaderm™ (3 M, Bracknell, UK) and kinesiology tape (KT Health, American Fork, USA). For procedures where anaesthesia was required, 2–4% isoflurane in oxygen was used. On day 1, blood samples were taken *via* tail vein bleeding at t = 1, 2, 4 and 6 h. Subsequent blood samples were collected at 1, 2, 3, 7, 14, 21, 28 and 35 days after treatment with either IM injection or MAPs.

2.19. Drug extraction from plasma

Study samples, which were composed of whole rat blood, were taken in 1.5 mL centrifuge tubes containing of heparin (10 μL) and centrifuged at 1509 *g* for 15 min (4 °C) to separate the plasma component. To extract CAB-Na from plasma, 100 μL of drug-containing plasma was mixed with 300 μL acetonitrile and vortexed at high speed for 15 min [39]. Then, the precipitated samples were centrifuged at 16,000 *g* for 15 min (4 °C) and the supernatant collected for analysis using the HPLC-MS method outlined in Section 2.21.

2.20. Analysis of pharmacokinetic (PK) parameters

Following quantification of CAB-Na in plasma samples, the delivery profile of CAB-Na was plotted *i.e.,* drug concentration in the plasma *versus* time. Subsequently, the pharmacokinetic parameters of this profile, namely the maximum CAB-Na concentration (C_{max}), the time needed to achieve C_{max} (T_{max}), half-life elimination time ($T_{1/2}$), mean residence time (MRT) and the area under the curve (AUC) were estimated using a non-compartmental PK model [40]. The relative bioavailability of CAB-Na in plasma after the administration of MAP compared to IM injection was calculated using Eq. (2).

$$FR = \frac{AUC \quad MAP \quad X \quad Dose \quad IM}{AUC \quad IM \quad X \quad Dose \quad MAP} \tag{2}$$

where, FR is the relative bioavailability, AUC MAP is the area under curve obtained from the integrated MAP2 formulation and AUC IM is the area under curve obtained from CAB LA (IM) injection.

2.21. HPLC-MS analysis for CAB-Na (in vivo analysis)

The development of a HPLC-MS method with isocratic elution was achieved using a HPLC with diode array detector (DAD), containing quaternary pump, multi-sampler, multi-column thermostat, attached to a single quadrupole mass spectrometer (API 6400, Agilent Technologies, UK) operated in a positive electrospray ionisation mode was utilised for species detection, with CAB and CAB-Na detected at *m/z* 406 and 428, respectively. The drying gas temperature was maintained at 300 °C, capillary voltage at 4 kV, nebuliser pressure at 15 psi and drying gas flow at 11 L/min. Chromatographic separation was achieved using a ZOR-BAX™ Eclipse XDB-C18 column (1.8 μm particle size, 50 mm length and 4.6 mm internal diameter), with column temperature kept at 40 °C. The mobile phase used was composed of 70% *v*/v ACN and 30% v/v ultra-purified water containing 0.1% v/v formic acid. The solvent flow rate was held at 0.3 mL/min for 6 min, and 10 μL of the sample injection volume [34].

2.22. Statistical analysis

Where applicable, the data was interpreted using one way analysis of variance (ANOVA) along with the Turkey-Kramer *post hoc* test (Graph-Pad Prism® software, version 9.1.0, San Diego, California, USA). In all cases, *p* < 0.05 denoted significance. Linear regression was applied for solubility studies using GraphPad Prism® software where *p* > 0.0037 denoted significance. Non-compartmental pharmacokinetic profile parameters were evaluated using the PKSolver add-in program in

Microsoft Excel™ (Microsoft Corporation, USA).

3. Results and discussion

3.1. Microscopic analysis of HF-MAPs

The morphology of formulated HF-MAPs was analysed using both digital light microscopy and SEM (Fig. 1). The chosen MN geometry was an 11 × 11 array (total MNs per array = 121) with MNs that were 900 μm high, composed of a pyramidal tip (600 μm) and cuboidal base (300 μm). Interspacing of MNs was 300 μm and the theoretical needle volume of each array was 5.45 mm^3 [32]. In this work, two HF-MAP types were investigated, namely the "Super-swelling" MAP1 formulation (Fig. 1A) and the PVA/PVP MAP2 formulation (Fig. 1B).

3.2. Swelling studies of crosslinked MAPs

Swelling studies were conducted to evaluate the capacity of swelling for MAP1 ("Super-swelling") and MAP2 (PVA-PVP) formulations. This work served as an indicator for the capacity of each type of cross-linked hydrogel to absorb interstitial fluid and swell when inserted into the skin [27]. As water containing 5% *w/w* HP-β-CD was used as the receiver compartment media during *ex vivo* skin deposition studies, it was also used here as the swelling media. It can be seen in Fig. 2 that the "Super swelling" formulation based on Gantrez® S-97 had a swelling capacity that was approximately 9-fold greater than the PVA/PVP hydrogel. Anjani et al. reported similar swelling profiles for both hydrogel formulations when analogous swelling studies were performed in PBS (pH 7.4) [28]. An important observation during this study was that MAPs prepared from the "Super swelling" formulation became structurally weak after approximately 30 min of swelling, whereas, PVA/PVP MAPs remained intact throughout the duration of the study.

3.3. Mechanical characterisation of HF-MAPs

The ability of HF-MAPs to penetrate and insert into neonatal porcine skin was examined using OCT, as described previously [34]. Analysis of the OCT images obtained (Fig. 3) demonstrated that the penetration depth of MNs from MAP1 and MAP2 were 608.15 ± 43.95 μm for MAP1 and 724.41 ± 32.05 μm, respectively. These insertion depth values were
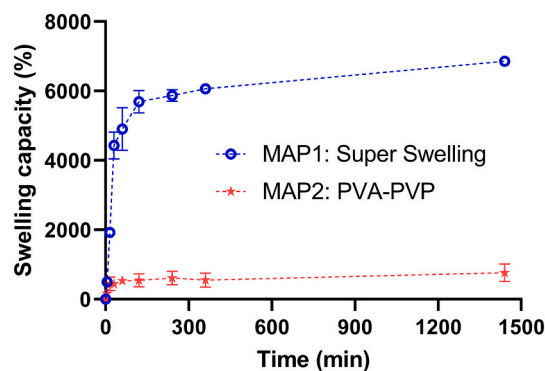
Fig. 2. Percentage swelling capacity of MAP1 and MAP2 in water containing 5% *w/w* HP-β-CD (mean ± S.D., *n* = 3).

higher than values previously reported [27,28]. A possible explanation for this could be related to the geometry of the MNs used in this study *i. e.,* cuboidal bases and pyramidal tips. This MN geometry may enhance skin penetration, compared to those that are conically shaped, due to the sharper edges of the cuboidal base more readily breaching the *stratum corneum* [41]. Additionally, it can be assumed that all MAPs were inserted accounting for approximately 68% and 80% of MAP height for MAP1 and MAP2, respectively.

These results have demonstrated that both MAP1 and MAP2 formulations have the capacity to effectively penetrate the *stratum corneum* (10–20 μm), excluding soles of feet and the palms (400–600 μm) [42]. The viable epidermis in humans, which is 100 μm thick, makes up the next layer of skin [42]. Beyond the epidermis is the dermis, a roughly 1200 μm thick where the majority of systemic drug are absorbed and it occurs due to the high level of vascularization in this layer [42]. The results from the simulated skin insertion studies suggest the ability of MAPs 1 and 2 of penetrating an approximate depth of 600–725 μm, which indicated the capability of the formulated MAPs to easily bypass the *stratum corneum* (~20 μm) as well as epidermis (~100 μm) layers. Provided that the loaded drug can successfully diffuse through the cross-linked hydrogel, it is reasonable to assume that drug deposition in the dermal layer, followed by systemic absorption *via* the dermal micro-circulation, would occur [31].
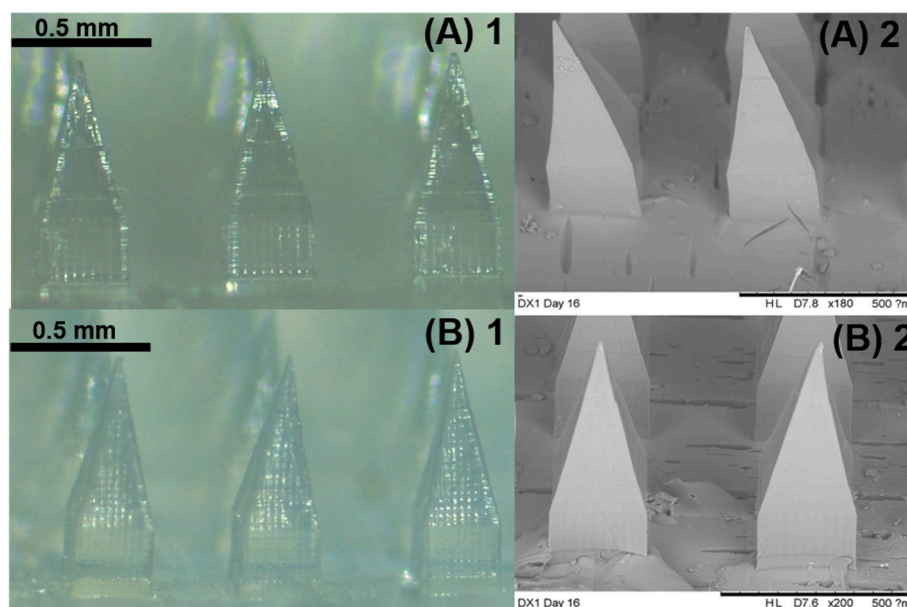
Fig. 1. Digital light microscope images of HF-MAPs: **(A)1** - MAP1 x8 magnification, **(B)1** - MAP2 x8 magnification, **(A)2** - MAP1 x35 magnification and **(B)2** - x35 magnification. SEM images of HF-MAPs:
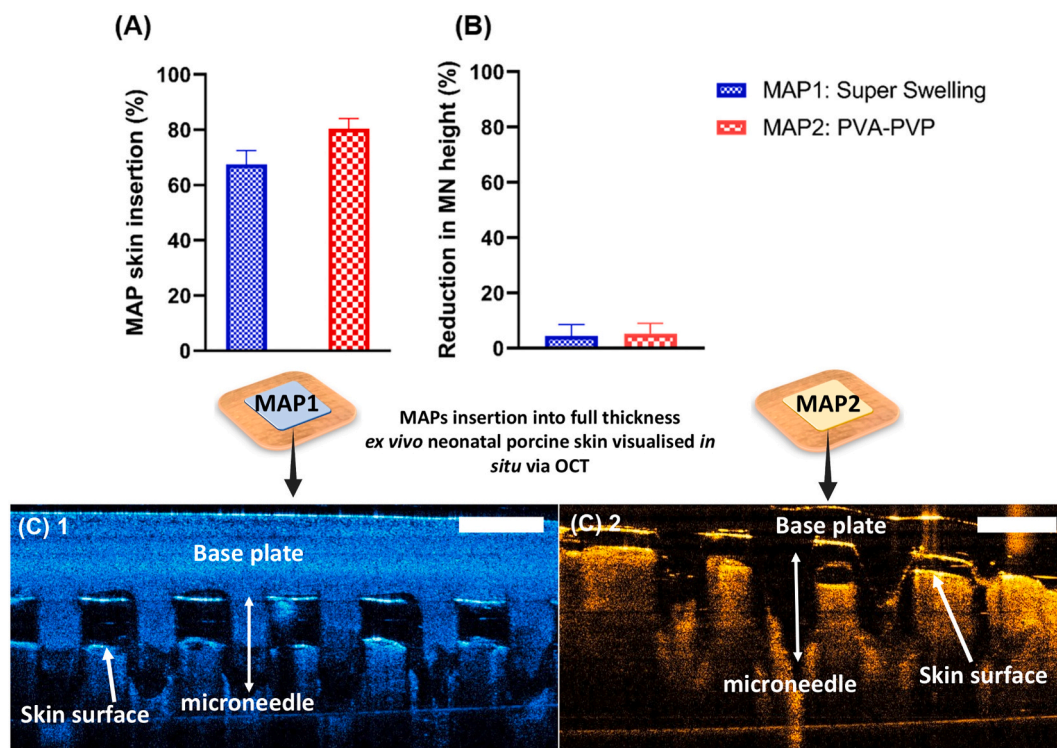
Fig. 3. (A) Percentage insertion of MNs on formulated HF-MAPs into full-thickness skin at a force of 32 N/ 30 s/array (means ± SD., n = 5). **(B)** Reduction in MN height (%) noted following compression onto an aluminum block (32 N/ 30 s/ array) (means + S.D., n = 5). **(C)** Representative OCT images of HF-MAPs inserted in full-thickness neonatal porcine skin - **(C) 1** = MAP1 and **(C) 2** = MAP2 (The scale bars represent a length of 500 μm).

To ensure penetration of the *stratum corneum* and subsequent drug deposition into lower layers of the skin, MNs should be strong enough to puncture the skin without breaking [40]. The height reduction after compression force application of HF-MNs was evaluated by compressing HF-MAPs using a force of 32 N/ 30 s and calculating the percentage MN height reduction (Fig. 3 (B)). Observed percentage MN height reduction was 4.57 ± 1.39% and 5.26 ± 1.55% for MAP1 and MAP2, respectively. These values were consistent with those previously reported and confirmed the suitability of both formulations in terms of mechanical strength [28,43].

3.4. Rationalisation of CAB-Na/HP-β-CD inclusion complex formation and tablet characterisation

The first objective of this work was to formulate a water-soluble drug reservoir using biocompatible material that would enhance the solubility of CAB-Na. Various surfactants and polymers were tested to improve CAB-Na solubility. However, only HP-β-CD was able to solubilise CAB-Na successfully (Table S1). To examine the relationship between the concentration of HP-β-CD and the observed solubility enhancement, an excess of CAB-Na was added to aqueous solutions containing increasing different concentrations of HP-β-CD. Fig. 4 (A) illustrates the influence of CD concentration on the aqueous solubility of CAB-Na. A linear relationship existed between the two components *i.e.,* as the concentration of HP-β-CD was increased, the solubility of the drug also increased. From this data, it was then possible to estimate the ratio of HP-β-CD to CAB-Na required for successful inclusion complex formation using Eqs. (3) and (4), where the moles of CAB-Na and HP-β-CD were compared.

$$CAB \quad Na + HP\beta CD = CAB \quad Na - HP\beta CD \tag{3}$$

$$K = \frac{[CAB \quad Na - HP\beta CD]}{[CAB \quad Na]x[HP\beta CD]} \tag{4}$$

Based on Eqs. (3) and (4), the stoichiometric molar ratio between CAB-Na: HP-β-CD was found to be 1:1 in the inclusion complex (Fig. 4 (B)). This indicated that successful inclusion complex formation occurred between one molecule of CAB-Na and one molecule of HP-β-CD. Furthermore, based on the maximum observed solubility of CAB-Na (8.6 ± 0.22 mg/mL), which occurred in the solution containing HP-β-CD 20% w/w, an approximate 19-fold solubility enhancement could be ascribed to the formation of CAB-Na/HP-β-CD inclusion complexes. Of those tested, 20% w/w of HP-β-CD was carefully chosen as the most suitable concentration for the formation of CAB-Na/HP-β-CD inclusion complexes, as it demonstrated the greatest improvement in the solubility of the drug. Higher CD concentrations were not investigated, as they would greatly increase the bulk of the final dosage form, which may then have affected the performance of the final integrated MAP device.

To obtain CAB-Na/HP-β-CD inclusion complexes in the solid state, an aqueous solution of HP-β-CD (20% w/w) was saturated with CAB-Na and the resultant solution was then lyophilised. By removing water in this manner, the remaining powder consisted of CAB-Na complexed with HP-β-CD in a mass ratio of 4:96 w/w. To convert this lyophilised powder into a suitable drug reservoir for use with a HF-MN array, it was processed into directly compressed tablets as depicted in Fig. 4(C) and (D). Each tablet was composed of 250 mg of CAB-Na/HP-β-CD inclusion complex powder (drug content = 10.32 ± 0.03 mg or 4.22 ± 0.03%), measured 13 ± 0.11 mm in diameter, and had a thickness of 1.40 ± 0.02 mm. Moreover, the formulated reservoir was distinctly hygroscopic in nature - dissolving in approximately 90 s during dissolution studies.

3.5. X-ray powder diffraction (XRD) analyses

The crystalline nature of CAB-Na, HP-β-CD, physical mixture (PM) of CAB-Na and HP-β-CD PM, and powdered CAB-Na/HP-β-CD inclusion complexes were examined using XRD (Fig. 5). The diffractogram obtained for CAB-Na was typical of a crystalline substance, with intense peaks observed at 7.3, 19.0, 20.6 and 24.1° theta [44]. When compared
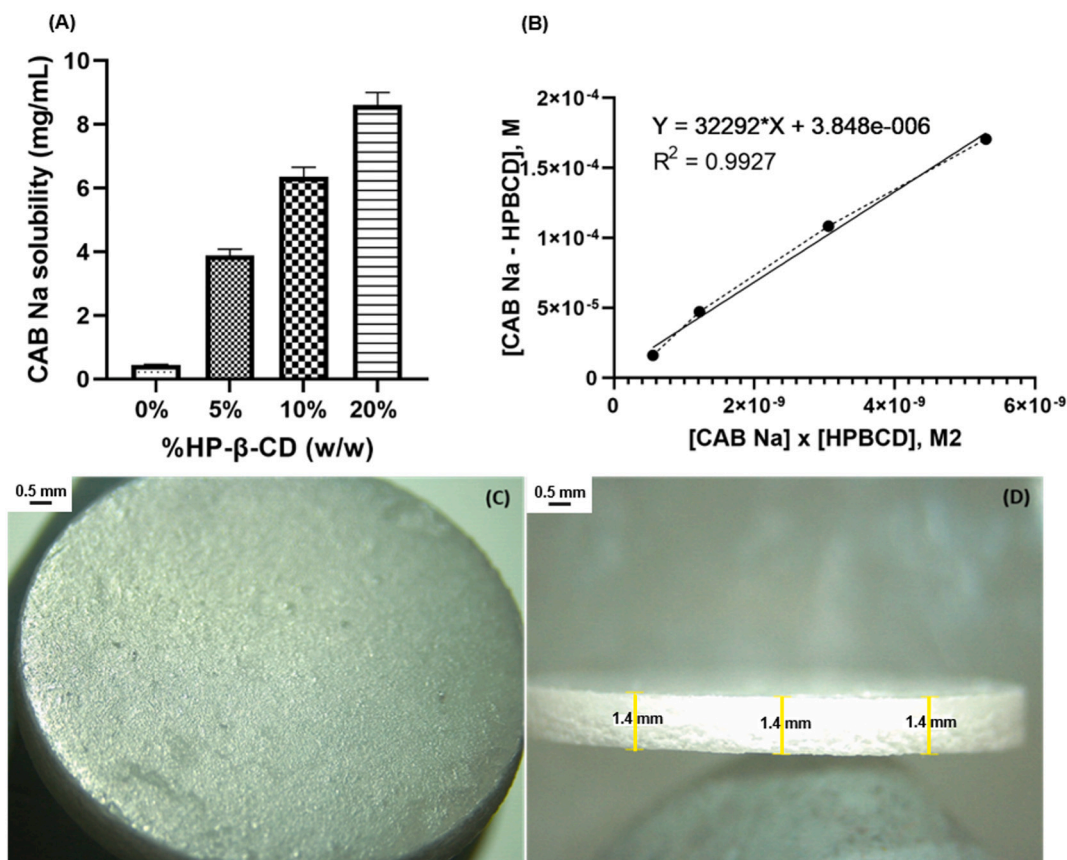
Fig. 4. (**A**) Observed solubility of CAB-Na when solubilised in aqueous condition containing HP-β-CD at concentrations varying from 5 to 20% w/w (means + S.D., *n* = 12). (**B**) Solubilisation of CAB-Na in HP-β-CD solutions. Solubility of CAB-Na is linearly reliant on the concentration of HP-β-CD. The proportion found for the inclusion complex was 1:1 (CAB-Na: HP-β-CD) stoichiometrically. (C) Microscopic image of CAB-Na/HP-β-CD tablet upper surface and (D) Microscopic image of CAB-Na/HP-β-CD tablet lateral surface.

to the diffractogram for HP-β-CD, which had two broad peaks at 11.9 and 19.9° theta and was bereft of any intense crystalline peaks, it was evident that the CD demonstrated extensive amorphous content [45]. The XRD of the CAB-Na and HP-β-CD physical mixture resulted in a diffractogram overlap with the patterns of these individual components, verifying that there was no chemical interaction between CD and drug, and that both components had retained their original physical characteristics. Finally, analysis of CAB-Na/HP-β-CD inclusion complexes provided a diffractogram that was similar to that of HP-β-CD alone and revealed a disappearance of the intense crystalline peaks observed during analysis of the pure drug. This finding indicated the conversion of the crystalline structure of CAB-Na to one that was amorphous, most likely due to successful CD/drug inclusion complex formation [45].

3.6. NMR and FTIR results

The complexation that took place between HP-β-CD and CAB-Na was confirmed by monitoring the proton chemical shifts using ^{1}H NMR. ^{1}H NMR spectra of the host HP-β-CD (host) and CAB-Na (guest) molecules and corresponding complexes were compared as shown in Fig. 6 (A, B and C). Upon complexation, it was clear that some degree of Δδ (proton chemical shift) had occurred for H-3 and H-5. These are the protons that reside within the cavity of the CD. In the presence of aromatic molecules such as those present on CAB-Na, the effect of resonance would induce an anisotropic effect on the H-3 and H-5 protons, resulting in proton chemical shifts, Δδ [46]. In addition, by monitoring the degree Δδ between H-3 and H-5, it can be deduced that there was partial or complete drug inclusion into the CD [47]. Table 3 shows that Δδ for H-5 > H-3, indicating total drug inclusion into the HP-β-CD cavity. In addition, FTIR

analysis was also conducted to complement the data obtained *via* ^{1}H NMR about the chemical interaction between HP-β-CD and CAB-Na. It can be seen from the FTIR analysis in Fig. 6 (D), that a broad peak at 1028 cm^{-1} was observed for the CAB-Na/HP-β-CD complex. This was not apparent for free HP-β-CD and CAB-Na + HP-β-CD physical mixture. The broad peak at 1028 cm^{-1} was assigned to the C-O stretching vibrations of the cyclodextrin molecule when complexation occurs between the cyclic oligosaccharides and CAB-Na [48]. The interaction between CAB-Na and HP-β-CD to form the complex of inclusion occurred in the H subjacent (CAB-Na) to the OH (HP-β-CD), clearly represented at 3363 cm^{-1} band and confirmed at the 1371 cm^{-1} stretching, suggesting a hydrogen bond interaction between CAB-Na and HP-β-CD occurred [48]. Collectively the ^{1}H NMR analysis in tandem with FTIR spectra indicate successful CAB-Na complexation withing the ring of HP-β-CD.

3.7. Ex vivo drug deposition studies

The results shown in Table 4 and Fig. 7 illustrate the amount of CAB-Na delivered into and through neonatal porcine skin (full-thickness, ∼ 2 mm) after application of previously formulated CAB-Na/HP-β-CD tablets in combination with MAP1 and MAP2. Additionally, the delivery of CAB-Na from CAB-Na/HP-β-CD tablets without MAPs was investigated *i. e.,* tablets were applied directly to the skin. As detailed in Table 2, the drug content of the formulated CAB-Na/HP-β-CD tablets was approximately 10,325 ± 35.82 μg per tablet.

CAB delivery from the integrated MAP1 containing the CAB-Na/HP-β-CD as a drug reservoir (Fig. 8 (A)) was evaluated employing a Franz-cell set-up with full-thickness neonatal porcine skin. The total drug delivered was 208.9 ± 51.93 μg/0.5 cm^2/CAB-Na/24 h, corresponding
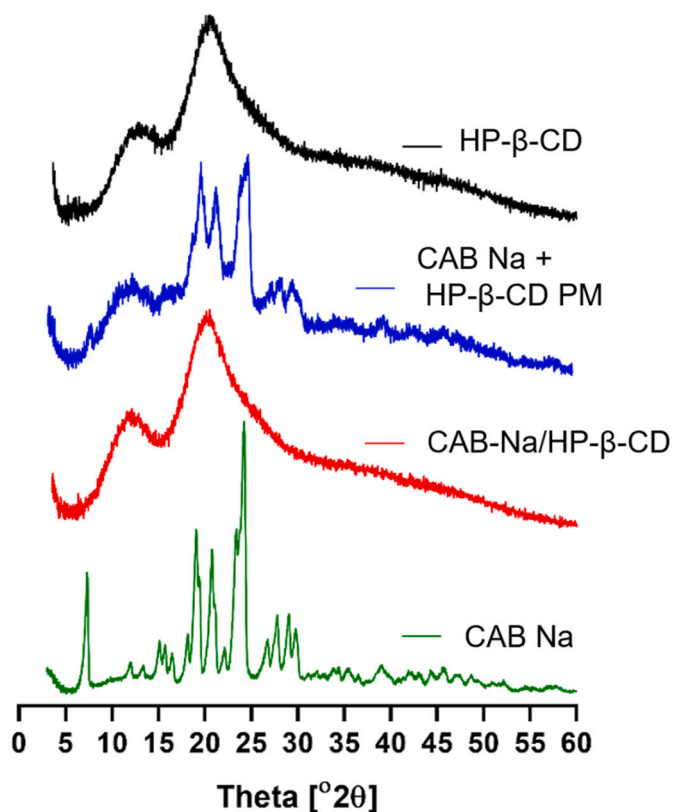
Fig. 5. XRD diffractograms of CAB-Na, HP-β-CD, a physical mixture of CAB-Na and HP-β-CD (CAB-Na + HP-β-CD PM), and CAB-Na/HP-β-CD inclusion complexes.

to $2.02 \pm 0.52\%$. The extent of drug deposited in the skin after 24 h was 141.63 ± 40.32 μg ($1.41 \pm 0.40\%$) of CAB-Na per 0.5 cm^2 of skin, while 67.27 ± 11.61 μg ($0.67 \pm 0.11\%$) of CAB-Na permeated across the skin into the receptor compartment of the Franz-cells within 24 h.

For MAP1, most of the drug was deposited into the swollen polymeric network, from where 6650 ± 395.35 μg ($64.40 \pm 4.99\%$) of unreleased CAB-Na was recovered. The recovery from donor compartments and skin surfaces was also studied, with a combined total of $2.64 \pm 0.28\%$ of CAB-Na found here.

In the same *ex vivo* skin delivery experiment, MAP2 was able to deliver 456.60 ± 90.51 μg/0.5 cm^2 of CAB-Na after 24 h. This corresponded to $4.41 \pm 0.65\%$ of total CAB-Na loaded and was 2.23-fold greater than observed with MAP1. From this total delivery, 324.00 ± 38.04 μg/0.5 cm^2 ($3.13 \pm 0.43\%$) was deposited in the skin and 132.60 ± 52.47 μg/0.5 cm^2 ($1.28 \pm 0.22\%$) permeated through the skin. Regarding recovery data, a large amount of drug was also found in the swollen polymeric matrix of MAP2, accounting for 4407 ± 650.62 μg ($42.68 \pm 8.22\%$) of CAB-Na. In addition, a total of 4542 ± 1028.71 μg ($43.99 \pm 12.99\%$) of CAB-Na was recovered from the donor compartment and skin surface.

The third group tested in this experiment was the CAB-Na/HP-β-CD tablet applied to intact skin without MAP application ('No MAP'). Drug deposition in the skin with the No MAP group was greatly reduced, with 21.13 ± 2.30 μg ($0.20 \pm 0.02\%$) delivered after 24 h. For this group, the drug was not detected in the receiver compartment, highlighting the importance of MAP application to enhance the intradermal and transdermal delivery of CAB-Na. Accordingly, CAB-Na was only recovered from the donor compartment and skin surface after 24 h, where a total of 6775 ± 5.68 μg ($65.16 \pm 0.05\%$) of CAB-Na was found.

The successful delivery of CAB-Na *via* MAP2 can be explained by crosslinking difference between the two formulations [28]. As reported by Anjani *et al* [28], the super-swelling MAP, formulated with Gantrez®

S97, PEG 10,000 and Na_2CO_3 has a polymer network formed with bigger pores when compared with the PVA-PVP formulation. In addition, there is the possibility that Gantrez® S97 interacts strongly with the drug and/ or the CD as well, explaining a marked difference observed between samples from MAP1 and MAP2 after the skin deposition experiment. Fig. 8 (B) shows the MAP1 (super-swelling) surface, with a large amount of drug deposited into the MAP1 polymeric network ($\sim 64\%$), which resulted in the formation of holes in the tips after the saturation of the hydrogel network with CAB-Na/HP-β-CD complex. Fig. 8 (C) shows the image of the skin surface that was in contact with MAP1, after 24 h of experiment. It is possible to see the drug precipitated on the skin surface. This phenomenon occurred due to the super-swelling formulation's high capacity of swelling and getting out of the skin after some period, which explains the amount of drug accumulated on the skin surface. Unlike MAP1, MAP2 remained fully formed, with no apparent precipitation of the drug in the polymeric network - Fig. 8 (D) -, and the skin surface (E) was not covered with the drug.

The CAB-Na/HP-β-CD complex tablet was able to release the hydrophobic CAB-Na through the cross-linked HF-MAPs, because these types of hydrogels are inherently aqueous in nature [27,43]. The water-soluble CAB-Na/HP-β-CD complex was capable of delivering the hydrophobic CAB-Na through the HF-MAPs due to the drug solubility enhancement achieved by complexation using HP-β-CD.

3.8. In vivo studies

Pharmacokinetic investigation of the delivery of CAB-Na from the formulated integrated MAP (MAP2 arrays combined with CAB-Na/HP-β-CD) tablet reservoirs were carried out on female Sprague-Dawley rats (aged between 8 and 12 weeks). The delivery of this anti-HIV therapeutic using MAP technology was compared to that of an FDA-approved long-acting nanosuspension of CAB (CAB-LA – average particle size = 200 nm) delivered *via* IM injection. The aim of this study was to deduce if minimally invasive HF MAP-mediated delivery using the formulated MAP device was a suitable alternative to the marketed injectable formulation. After removing MAP2, we observed no inflammation or erythema at the side application as previously reported when applied in the human skin (*in vivo*) [25,49]. Fig. 9 and Table 5 depict the pharmacokinetic profile of the delivery of CAB-LA administered *via* IM injection and that of CAB-Na delivered *via* MAPs.

The observed C_{max} for the CAB LA (IM) group was 43.76 ± 5.36 μg/ mL and was achieved after 6 days (T_{max}). The C_{max} observed following treatment with the formulated MAP device was 58.98 ± 9.95 μg/mL, with a T_{max} of 3 days. Exposure of rats to CAB was estimated using AUC as a parameter. The AUC_{0-28} values for the IM and MAP groups were 644.76 ± 55.43 μg/mL*day and 529.58 ± 86.42 μg/mL/day, respectively. Interestingly, the AUC values between these groups were not statistically different ($p > 0.05$). The MRT following administration of CAB-Na *via* MAPs intradermally was approximately 10 days (9.71 ± 0.48 days), whereas this value was just over 17 days for CAB-LA administered *via* IM. Additionally, the relative bioavailability of CAB following MAP administration was compared to IM injection, which revealed a bioavailability of $4.9 \pm 0.8\%$. Crucially, despite the observed differences in several pharmacokinetic parameters between the two groups, both cohorts demonstrated statistically similar plasma concentrations across the 28-day study ($p > 0.05$). Considering that the therapeutic plasma concentration of CAB ranges from 0.664 μg/mL ($4 \times$ PA-IC$_{90}$) to 0.1664 μg/mL (PA-IC$_{90}$) [34,48], the present study shows that the formulated MAP device was able to deliver CAB at $4\times$ concentrations above the clinically-relevant plasma protein-adjusted concentration. This plasma level inhibits virus replication by 90% ($4 \times$ PA-IC90), guaranteeing the drug release into tissues at relevant concentrations and consequently maintaining therapeutic levels of CAB *in vivo* for 28 days for HIV prevention [34,48]. Considering the observed plasma concentration at the 28 day time point, which was approximately 22-fold higher than the PA-IC$_{90}$, additional *in vivo* investigation is necessary to
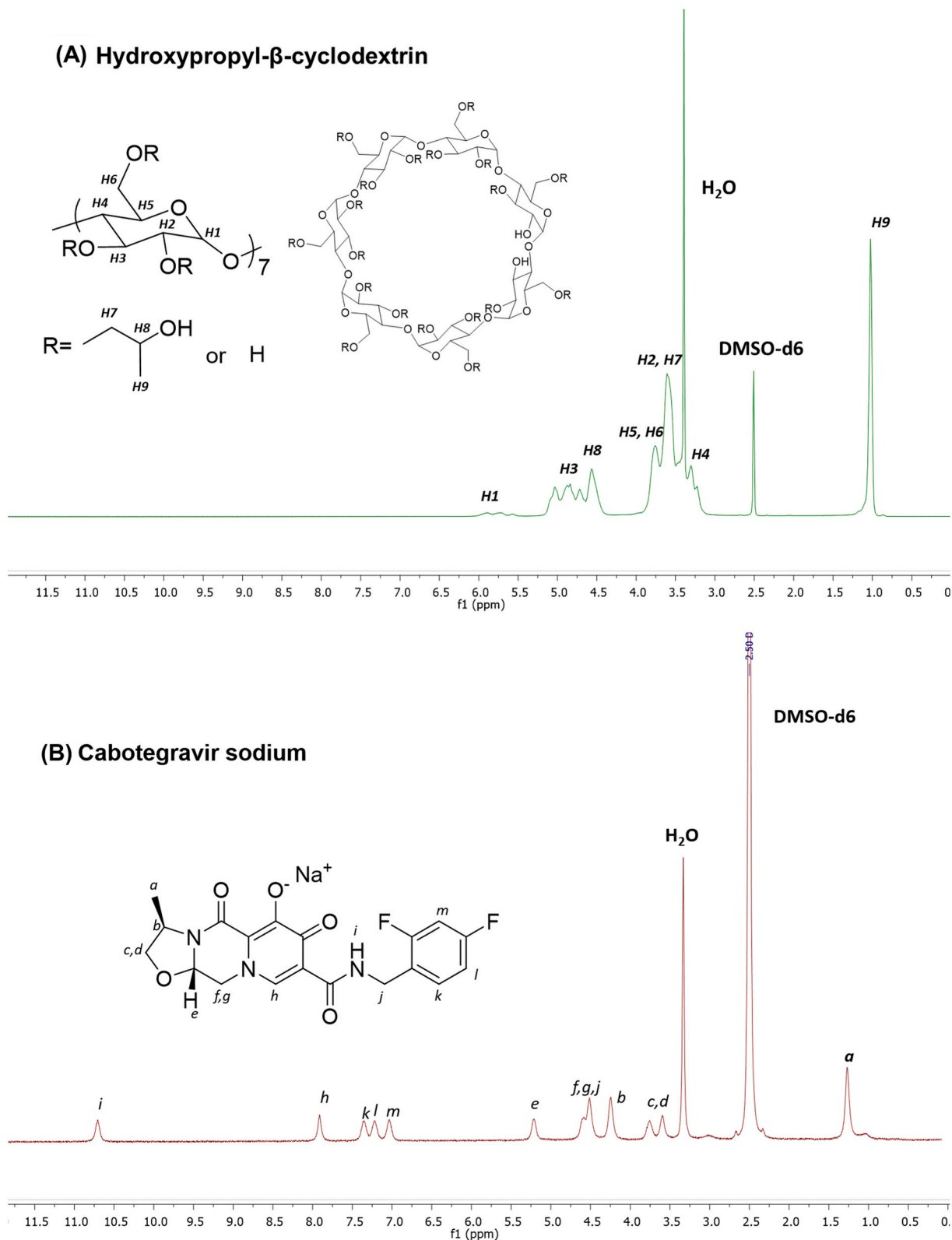
Fig. 6. Proton nuclear magnetic resonance (^{1}H NMR) spectra of (A) HP-β-CD. Proton nuclear magnetic resonance (^{1}H NMR) spectra of (B) Cabotegravir sodium and (C) CAB-Na/HP-β-CD Complex; (**D**) FTIR spectra of CAB-Na, CAB-Na/HP-β-CD Complex, a physical mixture of CAB-Na and HP-β-CD (CAB-Na + HP-β-CD PM) and HP-β-CD.

evaluate the formulation over longer time periods. The present data indicates the potential for sustained release of CAB-Na *via* HF-MAP for long-acting PrEP delivery, deserving further investigation. The initial

burst release from the formulated HF-MAP device may be attributed to the greatly enhanced solubility of CAB-Na brought about by inclusion complex formation. The rapid delivery and, subsequent, absorption of

(C) CAB Na/CD Complex
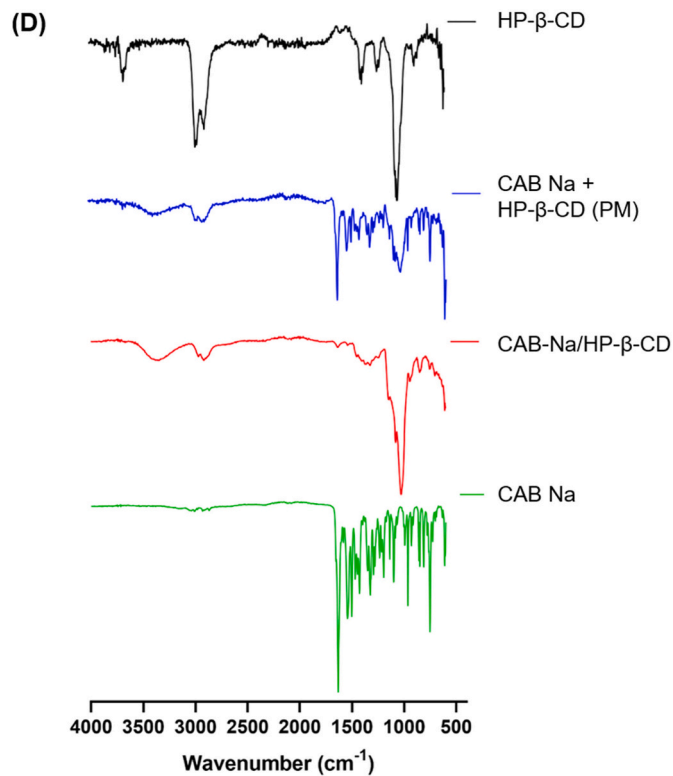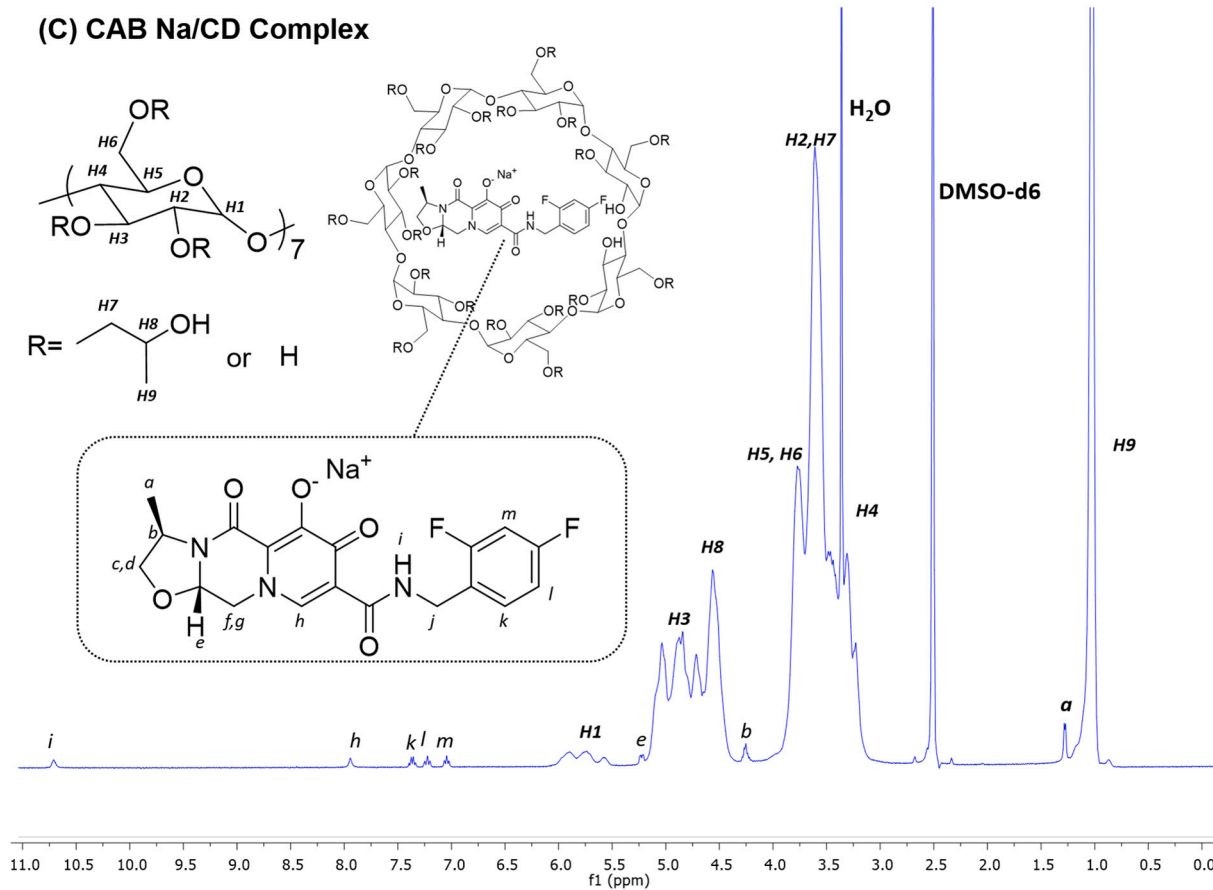
Fig. 6. (*continued*).
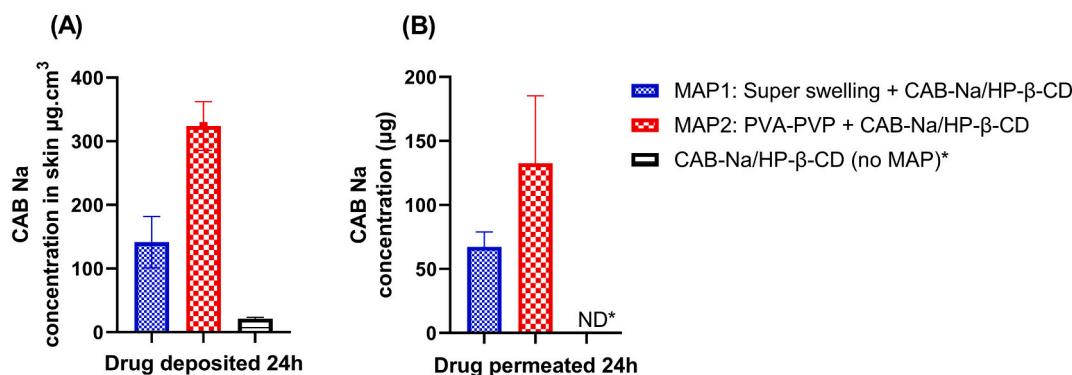
Fig. 7. (A) Concentration of CAB-Na deposited into full-thickness skin after 24 h **(B)** Concentration of CAB-Na permeated through the skin after 24 h. (Means ± S.D., *n* = 6) ND* = drug was not detected.

Table 2
Amount of CAB-Na present in lyophilised CAB-Na/HP-β-CD inclusion complex powder (100 mg) and in formulated CAB-Na/HP-β-CD tablets (250 mg) (means ± S.D., *n* = 12).

CAB-Na content		
Formulation	mg	% (w/w)
CAB-Na in 100 mg of CAB-Na/HP-β-CD	4.13 ± 0.02	4.13 ± 0.02
CAB-Na (Tablet 250 mg)	10.32 ± 0.03	4.22 ± 0.03

Table 3
^{1}H NMR chemical shift ($\Delta\delta$) data of HP-β-CD and the CAB-Na/HP-β-CD complexes. A $\Delta\delta = \delta$ (complex) - δ (free).

^{1}H-assingment	δ/ppm		$\Delta\,\delta$/ppm
	HP-β-CD	CAB-Na/HP-β-CD Complexes	
H-1	5.890	5.887	−0.003
H-2	3.601	3.601	0.000
H-3	4.832	4.833	0.001
H-4	3.295	3.292	−0.003
H-5	3.750	3.742	−0.008
H-6	3.750	3.742	−0.008
H-8	4.558	4.551	−0.007
H-9	1.018	1.019	−0.001

Table 4
Mass transfer of CAB-Na from formulated tablets using MAP1, MAP2 and No MAP. The percentage values (%, *w/w*) were calculated in relation to 10.3 mg of CAB-Na present in 250 mg CAB-Na/HP-β-CD tablet. (Means ± S.D., *n* = 6).

Type of MAP	MAP1 -"Super-Swelling"		MAP2 - PVA-PVP		No MAP	
CAB-Na	μg	%	μg	%	μg	%
Drug deposited skin/24 h	141.63 ± 40.32	1.37 ± 0.50	324.00 ± 38.04	3.13 ± 0.43	21.13 ± 2.30	0.20 ± 0.02
Drug permeated/ 24 h	67.27 ± 11.61	0.65 ± 0.02	132.60 ± 52.47	1.28 ± 0.22	ND	ND
Recovery MNs array	6650 ± 395.35	64.40 ± 4.99	4407 ± 650.62	42.68 ± 8.22	*	*
Recovery weight/ donor compartment	273.20 ± 20.05	2.64 ± 0.28	4542 ± 1028.71	43.99 ± 12.99	6775 ± 5.68	65.16 ± 0.05
Recovery total	7132 ± 442.02	69.07 ± 5.59	9405 ± 588.74	91.08 ± 7.43	6796 ± 7.22	65.82 ± 0.06

CAB-Na observed following MAP application provided a faster T_{max} and higher C_{max} compared to the slow releasing CAB LA IM injection. Encouragingly, the formulated MAP device also demonstrated an

Table 5
CAB pharmacokinetic parameters in animals and their corresponding dose based on the body weight-normalised, following administration of CAB-Na delivered *via* MAPs (MAP2 formulation) and CAB-LA administered *via* IM injection (Means ± S.D., *n* = 6).

Pharmacokinetic Parameters	CAB LA (IM)	CAB-Na (MAP2+CAB-Na/HP-β-CD tablet)
Applied dose (mg/rat)	2.5	40
Applied dose(mg/kg)	11.8 ± 0.5	189.4 ± 9.7
C_{max}(μg/mL)	43.76 ± 5.36	58.98 ± 9.95
T_{max}(day)	5.83 ± 2.05	2.83 ± 1.17
$C_{28\,days}$(μg/mL)	11.2 ± 3.3	3.6 ± 0.8
AUC_{0-28}(μg/mL*day)	644.76 ± 55.43	529.59 ± 86.42
AUC_{0-inf}	816.48 ± 106.83	559.94 ± 92.44
MRT (day)	17.27 ± 4.09	9.71 ± 0.48
$T_{1/2}$(day)	10.12 ± 2.73	5.79 ± 0.20
FR^*	1.00	0.049 ± 0.008

extended delivery profile. This could be attributed to the combination of rate-controlled drug delivery through a cross-linked hydrogel matrix and the formation of drug micro-depots in the skin following successful delivery. Upon delivery of drug/CD inclusion complexes to the dermal layer of the skin, the binding constant between CAB and HP-β-CD greatly influences drug release [48]. As a result, it is unlikely that all of the delivered inclusion complexes will remain intact, rather it is probable that at least some dissociate into CAB-Na and HP-β-CD [48]. This intradermal dissociation may lead to the formation of micro-depots of the poorly soluble drug CAB-Na in the skin, from which extended drug release occurs over a period of at least one month.

In this study, HF-MAPs have been successfully utilised for the long-acting delivery of the poorly soluble anti-HIV drug CAB. These MAPs, which absorb interstitial fluid from the skin upon application, swell to form an inserted hydrogel matrix *in situ* through which therapeutics can be delivered to the skin. Transcutaneous delivery in this manner is inherently well-suited for the delivery of hydrophilic molecules, due to the aqueous nature of a swollen hydrogel. However, the delivery of hydrophobic drugs using this technique has proven to be problematic [25,28]. Through the complexation of CAB-Na with the solubility enhancing oligosaccharide HP-β-CD and subsequent formulation into a soluble tablet reservoir, the previously elusive delivery of a hydrophobic compound *via* HF-MAPs was achieved. This finding will serve to expand the library of drugs deliverable using HF-MAPs to include those that display poor aqueous solubility.

Regarding the use of MAP technology to deliver anti-HIV therapeutics, only four drugs have been successfully delivered previously, rilpivirine (RPV) [50], etravirine [51], cabotegravir [34], and tenofovir alafenamide [18] using dissolving MAPs or long-acting implantable poly
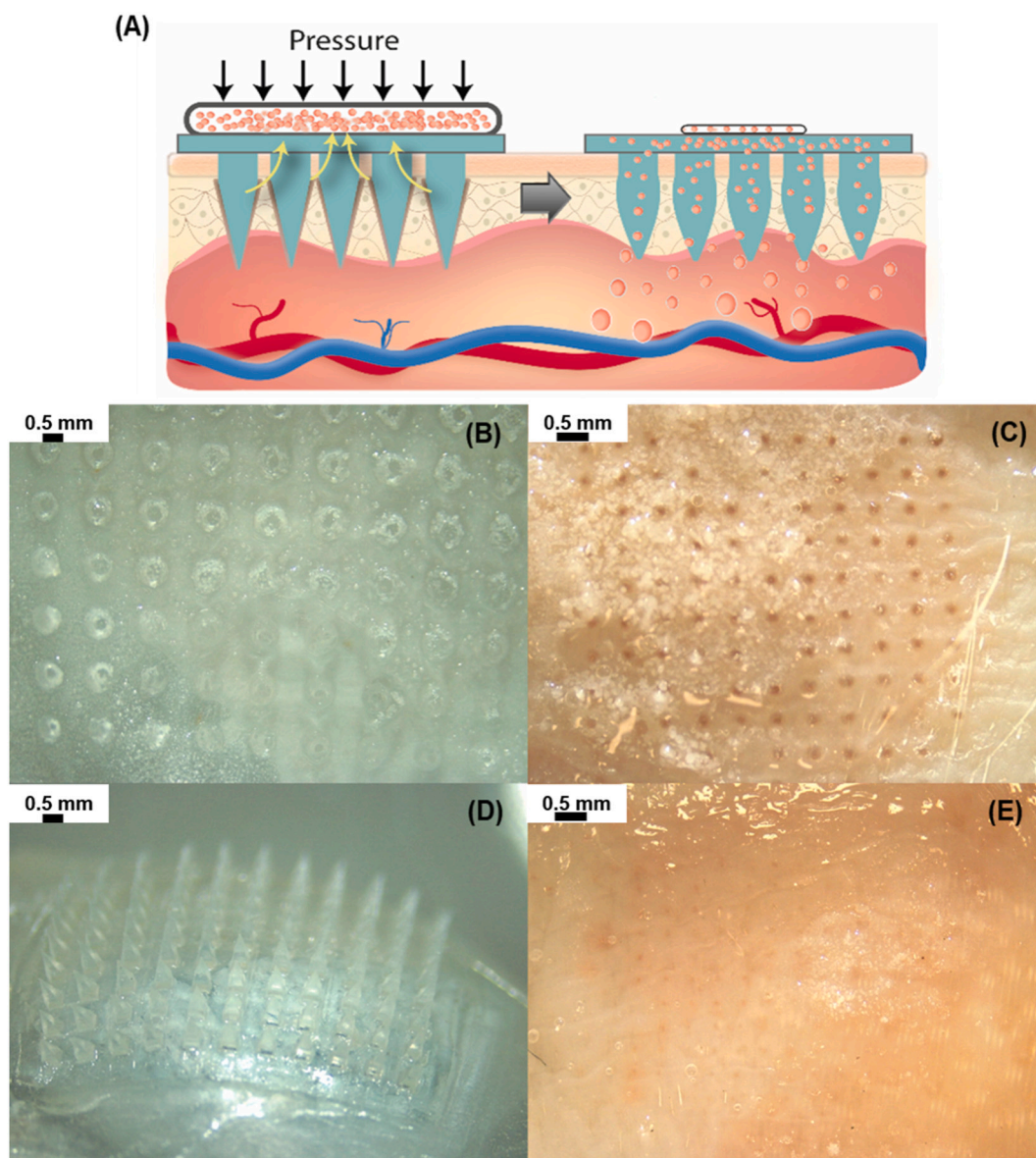
Fig. 8. (**A**) Schematic representation of HF-MAP mediated delivery of a drug from a tablet reservoir. Digital light microscopy images of (**B**) MAP1 after skin deposition experiment (x12.5 magnification), (**C**) skin surface where MAP1 was applied during skin deposition experiment (x12.5 magnification), (**D**) MAP2 after skin deposition experiment (x8 magnification), and (**E**) skin surface where MAP2 was applied during skin deposition experiment (x12.5 magnification).

(d,L-lactide-*co*-glycolide) (PLGA) MAPs [18,58]. In all cases, formulation and successful delivery in a long-acting manner was achieved by forming intradermal micro-depots in the skin using dissolving MAPs. To guarantee the successful delivery of a hydrophobic anti-HIV drug for the first-time using HF-MAPs, it was important to confirm their ability to penetrate the skin and maintain their swollen form after influx of interstitial skin fluid. In this work, a new MAP design which was comprised of individual MNs measuring 900 μm in height, with a cuboidal base (300 μm) and a pyramidal tip (600 μm), arranged in an 11 × 11 formation with 300 μm interspacing between MNs, was employed. The formulated MAPs were able to penetrate the skin and swell effectively without exhibiting expulsion from the skin [32]. The formulation MAP2 associated with drug reservoir CAB-Na/HP-β-CD had 5% relative bioavailability, corresponding to 500 μg of CAB-Na delivered per 0.5 cm^2 in 24 h from the drug reservoir. Similar amounts of drug were delivered in *ex vivo* experiment using Franz-cell set ups ($\sim$ 456.60 μg/0.5 cm^2/24 h) with full-thickness skin, reaffirming that the *in vitro* methodology to evaluate the new formulations can predict the expected

in vivo delivery.

Not only is the work reported here the first to deliver a hydrophobic compound *via* HF-MAPs, but it is also the first example of the delivery of an anti-HIV therapeutic using the same platform. Additionally, we have also demonstrated the successful delivery of a long-acting depot using HF-MAP for the first time. This phenomenon has not been reported previously and may hold great potential for the delivery of a numerous types of drug molecules for a range of indications. The recently FDA-approved CAB LA and RPV LA injections, which are the first and only marketed formulations that provide long-acting for HIV PrEP in adults [52]. Whilst these products represent a milestone in the evolution of HIV therapy, they require monthly or bimonthly administration by a trained healthcare professional using invasive IM injections. During Phase II and III clinical trials, >95% of individuals receiving CAB-LA *via* IM injection reported pain upon injection [53,56]. Furthermore, the generation of potentially-dangerous sharps waste is considered a major issue when dealing with a disease such as HIV, particularly in low and middle income settings, where the majority of HIV cases exist [21]. Therefore,
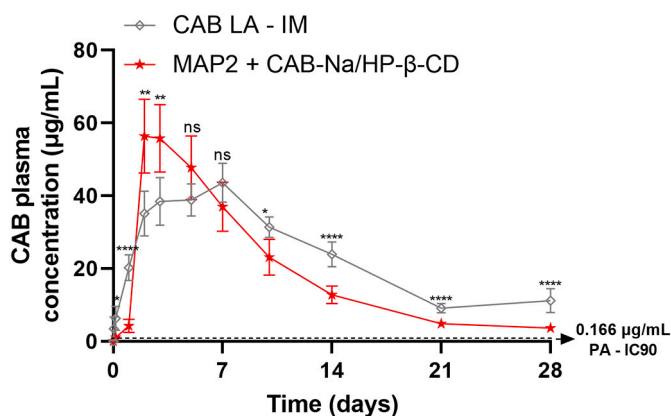
Fig. 9. Pharmacokinetic profiles following the administration of CAB-LA administered *via* IM injection and CAB-Na delivered *via* MAPs (MAP2 + CAB-Na/HP-β-CD) (Means ± S.D., $n = 6$). Statistical analysis using an unpaired *t*-test was used to compare groups at each time point. Accordingly, ns denoted no significant difference ($p > 0.05$), * denoted $p \leq 0.05$; ** denoted $p \leq 0.01$ and **** denoted $p \leq 0.0001$.

MAPs represent a promising alternative to the currently available oral and injectable treatments due to their ability to deliver HIV therapeutics at clinically relevant levels in a long-acting and minimally-invasive manner, without generating infectious sharps waste. Furthermore, MAPs are designed to be self-administered by the patient [54], thus relieving the burden placed on healthcare professionals in terms of treatment delivery.

4. Conclusion

This work describes, for the first time, the successful delivery of a poorly soluble anti-HIV drug using HF-MAPs. Cyclodextrin complexation has been proven to sufficiently solubilise the hydrophobic drug CAB-Na to facilitate its transdermal delivery across the aqueous channels of a swollen hydrogel MAP. This successful transdermal delivery can be attributed to the enhanced solubility exhibited by CAB-Na/HP-β-CD inclusion complexes which are able to traverse the swollen polymer matrix of an implanted HF-MAP. Following successful intradermal deposition, these complexes are sufficiently diluted in the skin and begin to spontaneously dissociate leading to intradermal drug depot formation and an extended drug release profile. The utilisation of effective HP-β-CD complexation teamed with the rate-controlled delivery of high drug loads provided by the HF-MAP platform facilitated the delivery of clinically relevant doses of CAB-Na in an *in vivo* setting over a 28-day period following a single administration. Further work is now required to optimise the formulated MAP device in terms of delivery efficiency. Nevertheless, the findings of this work demonstrate that the current long-acting delivery profile is similar to that of the FDA-approved CAB-LA (IM injection) marketed for PrEP and HIV treatment. Alternative minimally invasive delivery systems such as HF-MAPs have the potential to unlock benefits for those who are affected by HIV PrEP. Realisation of this potential will surely improve the quality of life of millions across the globe.

CRediT authorship contribution statement

Fabiana Volpe-Zanutto: Conceptualization, Data curation, Formal analysis, Funding acquisition, Investigation, Methodology, Project administration, Resources, Software, Validation, Writing – original draft, Writing – review & editing. **Lalitkumar K. Vora:** Data curation, Conceptualization, Formal analysis, Investigation, Methodology, Writing – review & editing. **Ismaiel A. Tekko:** Data curation, Formal analysis, Conceptualization, Investigation. **Peter E. McKenna:** Writing –

original draft, Writing – review & editing. **Andi Dian Permana:** Data curation, Formal analysis, Conceptualization, Writing – original draft. **Akmal H. Sabri:** Data curation, Methodology, Formal analysis, Visualization, Writing – original draft. **Qonita K. Anjani:** Investigation, Methodology, Formal analysis, Writing – original draft. **Helen O. McCarthy:** Investigation, Methodology. **Alejandro J. Paredes:** Writing – review & editing. **Ryan F. Donnelly:** Supervision, Resources, Funding acquisition, Writing – original draft, Writing – review & editing.

Appendix A. Supplementary data

Supplementary data to this article can be found online at https://doi.org/10.1016/j.jconrel.2022.06.028.

References

[1] R.K.R. Rajoli, Z.R. Demkovich, C. Flexner, A. Owen, M. Sic, Predicting pharmacokinetics of a tenofovir alafenamide subcutaneous implant using PBPK modelling, Antimicrob. Agents Chemother. (2020) 1–19, https://doi.org/10.1128/AAC.00155-20.

[2] UNAIDS, Global HIV & AIDS Statistics vol. 2, 2021. https://www.unaids.org/en/resources/fact-sheet (accessed August 11, 2021).

[3] W. World Health Organization, HIV/AIDS, 30 Novemb. 2021, 2021.

[4] W. World Health Organization, HIV/AIDS, 30 Novemb. 2021. https://www.who.int/news-room/fact-sheets/detail/hiv-aids, 2021 (accessed December 1, 2021).

[5] A.J. Paredes, I.K. Ramöller, P.E. McKenna, M.T.A. Abbate, F. Volpe-Zanutto, L.K. Vora, M. Kilbourne-Brook, C. Jarrahian, K. Moffatt, C. Zhang, I.A. Tekko, R.F. Donnelly, Microarray patches: breaking down the barriers to contraceptive care and HIV prevention for women across the globe, Adv. Drug Deliv. Rev. 173 (2021) 331–348, https://doi.org/10.1016/j.addr.2021.04.002.

[6] J. Ghosn, B. Taiwo, S. Seedat, B. Autran, C. Katlama, Seminar HIV, Lancet. 392 (2018), https://doi.org/10.1016/S0140-6736(18)31311-4.

[7] J.M. Molina, I. Charreau, B. Spire, L. Cotte, J. Chas, C. Capitant, C. Tremblay, D. Rojas-Castro, E. Cua, A. Pasquet, C. Bernaud, C. Pintado, C. Delaugerre, L. Sagaon-Teyssier, S. Le Mestre, C. Chidiac, G. Pialoux, D. Ponscarme, J. Fonsart, D. Thompson, M.A. Wainberg, V. Doré, L. Meyer, Efficacy, safety, and effect on sexual behaviour of on-demand pre-exposure prophylaxis for HIV in men who have sex with men: an observational cohort study, Lancet HIV 4 (2017) e402–e410, https://doi.org/10.1016/S2352-3018(17)30089-9.

[8] A.N. Nyaku, S.G. Kelly, B.O. Taiwo, Long-acting Antiretrovirals: where are we now? Curr. HIV/AIDS Rep. 14 (2017) 63–71, https://doi.org/10.1007/s11904-017-0353-0.

[9] R.K.R. Rajoli, D.J. Back, S. Rannard, C.F. Meyers, C. Flexner, A. Owen, M. Siccardi, In silico dose prediction for long-acting Rilpivirine and Cabotegravir administration to children and adolescents, Clin. Pharmacokinet. 57 (2018) 255–266, https://doi.org/10.1007/s40262-017-0557-x.

[10] T. Whitfield, A. Torkington, C. van Halsema, Profile of cabotegravir and its potential in the treatment and prevention of HIV-1 infection: evidence to date, HIV/AIDS - Res. Palliat. Care. 8 (2016) 157–164, https://doi.org/10.2147/HIV.S97920.

[11] C. Trezza, S.L. Ford, W. Spreen, R. Pan, S. Piscitelli, Formulation and pharmacology of long-acting cabotegravir, Curr. Opin. HIV AIDS 10 (2015) 239–245, https://doi.org/10.1097/COH.0000000000000168.

[12] S.L. Letendre, A. Mills, D. Hagins, S. Swindells, F. Felizarta, J. Devente, C. Bettacchi, Y. Lou, S. Ford, K. Sutton, J.S. Shaik, H. Crauwels, R. D'Amico, P. Patel, Pharmacokinetics and antiviral activity of cabotegravir and rilpivirine in cerebrospinal fluid following long-acting injectable administration in HIV-infected

adults, J. Antimicrob. Chemother. 75 (2020) 648–655, https://doi.org/10.1093/jac/dkz504.

[13] A.J. Paredes, I.K. Ramöller, P.E. McKenna, M.T.A. Abbate, F. Volpe-Zanutto, L. Vora, M. Kilbourne-Brook, C. Jarrahian, K. Moffatt, C. Zhang, I.A. Tekko, R. F. Donnelly, Microarray patches: breaking down the barriers to contraceptive care and HIV prevention for women across the globe, Adv. Drug Deliv. Rev. 173 (2021) 331–348, https://doi.org/10.1016/j.addr.2021.04.002.

[14] D. Rial-crestelo, A. Pinto-martínez, F. Pulido, D. Rial-crestelo, A. Pinto-martínez, F. Pulido, Expert Review of Anti-infective Therapy Cabotegravir and rilpivirine for the treatment of HIV Cabotegravir and rilpivirine for the treatment of HIV, Expert Rev. Anti-Infect. Ther. 00 (2020) 1–12, https://doi.org/10.1080/14787210.2020.1736561.

[15] Jennifer McLenon, Mary A.M. Rogers, The fear of needles: a systematic review and meta-analysis, J. Adv. Nurs. 75 (2019) 30–42, https://doi.org/10.1111/jan.13818.

[16] T. Hayashi, Y.J.F. Hutin, M. Bulterys, A. Altaf, B. Allegranzi, Injection practices in 2011-2015: a review using data from the demographic and health surveys (DHS), BMC Health Serv. Res. 19 (2019) 1–10, https://doi.org/10.1186/s12913-019-4366-9.

[17] F. Volpe-Zanutto, B. Fonseca-Santos, P.E. McKenna, A.J. Paredes, J.L. Dávila, M.T. C. McCrudden, M.M.P. Tangerina, M. Ceccheto Figueiredo, W. Vilegas, A. Brisibe, M. Akira D'vila, R.F. Donnelly, M. Chorilli, M.A. Foglio, Novel transdermal bioadhesive surfactant-based system for release and solubility improvement of antimalarial drugs artemether-lumefantrine, Biomed. Mater. 16 (2021), https://doi.org/10.1088/1748-605X/ac2885.

[18] A.J. Paredes, F. Volpe-Zanutto, L.K. Vora, I.A. Tekko, A.D. Permana, C.J. Picco, H. O. McCarthy, R.F. Donnelly, Systemic delivery of tenofovir alafenamide using dissolving and implantable microneedle patches, Mater. Today Bio. 13 (2022), 100217, https://doi.org/10.1016/j.mtbio.2022.100217.

[19] F.W. Hughes, G.D. Puoane, T.R. Clark, B.L. Wondwossen, T.L. Johnson, Prevalence and Predictors of Traditional Medicine utilization among persons living with AIDS (PLWA) on Antiretroviral (ARV) and Prophylaxis treatment in both rural and urban areas South Africa, Afr. J. Tradit Complement Altern Med. 9 (2012) 470–484.

[20] E. Sicuri, A. Vieta, L. Lindner, C. Sauboin, Economic costs of malaria in children in three Sub-Saharancountries: Ghana, Tanzania and Kenya, Tropical Med. Int. Health 16 (2011) 117. http://ovidsp.ovid.com/ovidweb.cgi?T=JS&PAGE=reference&D=emed13&NEWS=N&AN=70589204.

[21] F.V. Zanutto, E. Mcalister, M. Marucci, P. Tangerina, B. Fonseca-Santos, H. C. Salles, M.O. Souza, A. Brisibe, W. Vilegas, M. Chorilli, M. Akira D' Avila, R. F. Donnelly, M.A. Foglio, Semisynthetic derivative of *Artemisia annua*-loaded transdermal bioadhesive for the treatment of uncomplicated malaria caused by plasmodium falciparum in children, J. Pharm. Sci. 108 (2019) 1177–1188, https://doi.org/10.1016/j.xphs.2018.10.007.

[22] F. Volpe-Zanutto, L. Tiburcio, A. Dian, M. Kirkby, A.J. Paredes, L.K. Vora, A. P. Bonfanti, I. Charlie-silva, C. Raposo, M.C. Figueiredo, I.M.O. Sousa, A. Brisibe, R. F. Donnelly, M. Ann, F. Trindade, Artemether and lumefantrine dissolving microneedle patches with improved pharmacokinetic performance and antimalarial efficacy in mice infected with Plasmodium yoelii, J. Control. Release 333 (2021) 298–315, https://doi.org/10.1016/j.jconrel.2021.03.036.

[23] A.J. Paredes, F. Volpe-Zanutto, A. Dian Permana, A.J. Murphy, C.J. Picco, L. K. Vora, J.A. Coulter, R.F. Donnelly, Novel tip-loaded dissolving and implantable microneedle array patches for sustained release of finasteride, Int. J. Pharm. (2021), 120885, https://doi.org/10.1016/j.ijpharm.2021.120885.

[24] A.J. Paredes, P.E. McKenna, I.K. Ramöller, Y.A. Naser, F. Volpe-Zanutto, M. Li, M. T.A. Abbate, L. Zhao, C. Zhang, J.M. Abu-Ershaid, X. Dai, R.F. Donnelly, Microarray patches: poking a hole in the challenges faced when delivering poorly soluble drugs, Adv. Funct. Mater. 2005792 (2020) 1–27, https://doi.org/10.1002/adfm.202005792.

[25] R.F. Donnelly, T.R.R. Singh, M.J. Garland, K. Migalska, R. Majithiya, C. M. McCrudden, P.L. Kole, T.M.T. Mahmood, H.O. McCarthy, A.D. Woolfson, Hydrogel-forming microneedle arrays for enhanced transdermal drug delivery, Adv. Funct. Mater. 22 (2012) 4879–4890, https://doi.org/10.1002/adfm.201200864.

[26] L.K. Vora, K. Moffatt, I.A. Tekko, A.J. Paredes, F. Volpe-Zanutto, D. Mishra, K. Peng, R. Raj Singh Thakur, R.F. Donnelly, Microneedle array systems for long-acting drug delivery, Eur. J. Pharm. Biopharm. 159 (2021) 44–76, https://doi.org/10.1016/j.ejpb.2020.12.006.

[27] D. Ramadon, A.D. Permana, A.J. Courtenay, M.T.C. McCrudden, I.A. Tekko, E. McAlister, Q.K. Anjani, E. Utomo, H.O. McCarthy, R.F. Donnelly, Development, evaluation, and pharmacokinetic assessment of polymeric microarray patches for transdermal delivery of vancomycin hydrochloride, Mol. Pharm. 17 (2020) 3353–3368, https://doi.org/10.1021/acs.molpharmaceut.0c00431.

[28] Q.K. Anjani, A.D. Permana, Á. Cárcamo-Martínez, J. Domínguez-Robles, I. A. Tekko, E. Larrañeta, L.K. Vora, D. Ramadon, R.F. Donnelly, Versatility of hydrogel-forming microneedles in in vitro transdermal delivery of tuberculosis drugs, Eur. J. Pharm. Biopharm. 158 (2021) 294–312, https://doi.org/10.1016/j.ejpb.2020.12.003.

[29] A. Ryzhakov, T. Do Thi, J. Stappaerts, L. Bertoletti, K. Kimpe, A.R. Sá Couto, P. Saokham, G. Van den Mooter, P. Augustijns, G.W. Somsen, S. Kurkov, S. Inghelbrecht, A. Arien, M.I. Jimidar, K. Schrijnemakers, T. Loftsson, Self-assembly of Cyclodextrins and their complexes in aqueous solutions, J. Pharm. Sci. 105 (2016) 2556–2569, https://doi.org/10.1016/j.xphs.2016.01.019.

[30] C.W. Yong, C. Washington, W. Smith, Structural behaviour of 2-hydroxypropyl-β-cyclodextrin in water: molecular dynamics simulation studies, Pharm. Res. 25 (2008) 1092–1099, https://doi.org/10.1007/s11095-007-9506-y.

[31] R.F. Donnelly, M.T.C. McCrudden, A.Z. Alkilani, E. Larrañeta, E. McAlister, A. J. Courtenay, M.C. Kearney, T.R. Raj Singh, H.O. McCarthy, V.L. Kett, E. Caffarel-

Salvador, S. Al-Zahrani, A.D. Woolfson, Hydrogel-forming microneedles prepared from "super swelling" polymers combined with lyophilised wafers for transdermal drug delivery, PLoS One 9 (2014), https://doi.org/10.1371/journal.pone.0111547.

[32] A.S. Cordeiro, I.A. Tekko, M.H. Jomaa, L. Vora, E. McAlister, F. Volpe-Zanutto, M. Nethery, P.T. Baine, N. Mitchell, D.W. McNeill, R.F. Donnelly, Two-photon polymerisation 3D printing of microneedle Array templates with versatile designs: application in the development of polymeric drug delivery systems, Pharm. Res. 37 (2020) 174, https://doi.org/10.1007/s11095-020-02887-9.

[33] K.A. Higuchi, T. Connors, Phase-solubility techniques, in: C.N. Reilly (Ed.), Adv. Anal. Chem. Instrum., Wiley-Interscience, New York, NY, 1965, pp. 117–122.

[34] I.A. Tekko, L.K. Vora, F. Volpe-Zanutto, K. Moffatt, C. Jarrahian, H.O. McCarthy, R. F. Donnelly, Novel bilayer microarray patch-assisted long-acting Micro-depot Cabotegravir intradermal delivery for HIV pre-exposure prophylaxis, Adv. Funct. Mater. (2021) 2106999, https://doi.org/10.1002/adfm.202106999.

[35] J. Siepmann, N.A. Peppas, Higuchi equation: derivation, applications, use and misuse, Int. J. Pharm. 418 (2011) 6–12, https://doi.org/10.1016/j.ijpharm.2011.03.051.

[36] A.D. Permana, A.J. Paredes, F. Volpe-Zanutto, Q.K. Anjani, E. Utomo, R. F. Donnelly, Dissolving microneedle-mediated dermal delivery of itraconazole nanocrystals for improved treatment of cutaneous candidiasis, Eur. J. Pharm. Biopharm. 154 (2020) 50–61, https://doi.org/10.1016/j.ejpb.2020.06.025.

[37] A.J. Paredes, F. Volpe-Zanutto, A.D. Permana, A.J. Murphy, C.J. Picco, L.K. Vora, J. A. Coulter, R.F. Donnelly, Novel tip-loaded dissolving and implantable microneedle array patches for sustained release of finasteride, Int. J. Pharm. 606 (2021), 120885, https://doi.org/10.1016/j.ijpharm.2021.120885.

[38] R.F. Donnelly, M.J. Garland, D.I.J. Morrow, K. Migalska, T. Raghu, R. Singh, R. Majithiya, A.D. Woolfson, Optical coherence tomography is a valuable tool in the study of the effects of microneedle geometry on skin penetration characteristics and in-skin dissolution, J. Control. Release 147 (2010) 333–341.

[39] I.K. Ramöller, M.T.A. Abbate, L.K. Vora, A.R.J. Hutton, K. Peng, F. Volpe-Zanutto, I.A. Tekko, K. Moffatt, A.J. Paredes, H.O. McCarthy, R.F. Donnelly, HPLC-MS method for simultaneous quantification of the antiretroviral agents rilpivirine and cabotegravir in rat plasma and tissues, J. Pharm. Biomed. Anal. 213 (2022), 114698, https://doi.org/10.1016/j.jpba.2022.114698.

[40] A.D. Permana, A.J. Paredes, F.V. Zanutto, M.N. Amir, I. Ismail, M.A. Bahar, S. D. Sumarheni, R.F. Donnelly Palma, Albendazole nanocrystal-based dissolving microneedles with improved pharmacokinetic performance for enhanced treatment of cystic echinococcosis, ACS Appl. Mater. Interfaces 13 (2021) 38745–38760, https://doi.org/10.1021/acsami.1c11179.

[41] E.Z. Loizidou, N.T. Inoue, J. Ashton-Barnett, D.A. Barrow, C.J. Allender, Evaluation of geometrical effects of microneedles on skin penetration by CT scan and finite element analysis, Eur. J. Pharm. Biopharm. 107 (2016) 1–6, https://doi.org/10.1016/j.ejpb.2016.06.023.

[42] L.G.C. Burkhart, D. Morrell, Dermatological Pharmacology, in: B.C.K.L.L. Brunton, A.B. Chabner (Eds.), Goodman Gilman's Farmacol. Basis Ther., 12ª ed, McGraw-Hill Medical, New York, NY, 2012.

[43] E.M. Migdadi, A.J. Courtenay, I.A. Tekko, M.T.C. Mccrudden, M. Kearney, E. Mcalister, H.O. Mccarthy, R.F. Donnelly, Hydrogel-forming microneedles enhance transdermal delivery of metformin hydrochloride, J. Control. Release 285 (2018) 142–151, https://doi.org/10.1016/j.jconrel.2018.07.009.

[44] A. Adamer, Verena; Thaler, Crystalline Forms of Cabotegravir Sodium, WO 2018149608 (A1), 2018.

[45] D. Han, Z. Han, L. Liu, Y. Wang, S. Xin, H. Zhang, Z. Yu, Solubility enhancement of myricetin by inclusion complexation with heptakis-o-(2-hydroxypropyl)-β-cyclodextrin: a joint experimental and theoretical study, Int. J. Mol. Sci. 21 (2020) 1–11, https://doi.org/10.3390/ijms21030766.

[46] H.-J. Schneider, F. Hacket, V. Rudiger, H. Ikeda, NMR studies of Cyclodextrins and Cyclodextrin complexes, Chem. Rev. 2665 (1998), https://doi.org/10.1021/cr970019t.

[47] D. Greatbanks, R. Pickford, Cyclodextrins as chiral complexing agents in water, and their application to optical purity measurements, Magn. Reson. Chem. 25 (1987) 208–215, https://doi.org/10.1002/mrc.1260250306.

[48] F.P. Pons-Faudoa, A. Sizovs, N. Di Trani, J. Paez-Mayorga, G. Bruno, J. Rhudy, M. Manohar, K. Gwenden, C. Martini, C.Y.X. Chua, G. Varchi, M.A. Marzinke, A. Grattoni, 2-Hydroxypropyl-β-cyclodextrin-enhanced pharmacokinetics of cabotegravir from a nanofluidic implant for HIV pre-exposure prophylaxis, J. Control. Release 306 (2019) 89–96, https://doi.org/10.1016/j.jconrel.2019.05.037.

[49] R. Al-Kasasbeh, A.J. Brady, A.J. Courtenay, E. Larrañeta, M.T.C. McCrudden, D. O'Kane, S. Liggett, R.F. Donnelly, Evaluation of the clinical impact of repeat application of hydrogel-forming microneedle array patches, Drug Deliv. Transl. Res. 10 (2020) 690–705, https://doi.org/10.1007/s13346-020-00727-2.

[50] M.T.C. Mc Crudden, E. Larrañeta, A. Clark, C. Jarrahian, A. Rein-Weston, S. Lachau-Durand, N. Niemeijer, P. Williams, C. Haeck, H.O. McCarthy, D. Zehrung, R.F. Donnelly, Design, formulation and evaluation of novel dissolving microarray patches containing a long-acting rilpivirine nanosuspension, J. Control. Release 292 (2018) 119–129, https://doi.org/10.1016/j.jconrel.2018.11.002.

[51] S. Rojekar, L.K. Vora, I.A. Tekko, F. Volpe-Zanutto, H.O. McCarthy, P.R. Vavia, R. F. Donnelly, Etravirine-loaded dissolving microneedle arrays for long-acting delivery, Eur. J. Pharm. Biopharm. (2021), https://doi.org/10.1016/j.ejpb.2021.04.024.

[52] M.I. Murray, M. Markowitz, I. Frank, R.M. Grant, K.H. Mayer, K.J. Hudson, B. S. Stancil, S.L. Ford, P. Patel, A.R. Rinehart, W.R. Spreen, D.A. Margolis, Satisfaction and acceptability of cabotegravir long-acting injectable suspension for

prevention of HIV: patient perspectives from the ECLAIR trial, HIV Clin. Trials. 19 (2018) 129–138, https://doi.org/10.1080/15284336.2018.1511346.

[53] C. Orkin, K. Arasteh, M. Górgolas Hernández-Mora, V. Pokrovsky, E.T. Overton, P.-M. Girard, S. Oka, S. Walmsley, C. Bettacchi, C. Brinson, P. Philibert, J. Lombaard, M. St, H. Clair, S.L. Crauwels, P. Ford, V. Patel, R. Chounta, S. D'Amico, D. Vanveggel, A. Dorey, S. Cutrell, D.A. Griffith, P.E. Margolis, W. Williams, K. Y. Parys, W.R. Spreen Smith, Long-acting Cabotegravir and Rilpivirine after Oral induction for HIV-1 infection, N. Engl. J. Med. 382 (2020) 1124–1135, https://doi.org/10.1056/NEJMoa1909512.

[54] J.J. Norman, J.M. Arya, M.A. McClain, P.M. Frew, M.I. Meltzer, M.R. Prausnitz, Microneedle patches: usability and acceptability for self-vaccination against influenza, Vaccine. 32 (2014) 1856–1862, https://doi.org/10.1016/j.vaccine.2014.01.076.

[55] P. Ranjan Yadav, M. Iqbal Nasiri, L.K. Vora, E. Larrañeta, R.F. Donnelly, S. K. Pattanayek, D. Bhusan Das, Super-swelling hydrogel-forming microneedle based

transdermal drug delivery: Mathematical modelling, simulation and experimental validation, Int. J. Pharmaceutics 622 (2022) 121835, https://doi.org/10.1016/j.ijpharm.2022.121835.

[56] A. Rein-Weston, I. Tekko, L. Vora, C. Jarrahian, B. Spreen, T. Scott, R. Donnelly, D. Zehrung, LB8. Microarray Patch Delivery of Long-Acting HIV PrEP and Contraception, Open Forum Infectious Diseases 6 (2019) S996, https://doi.org/10.1093/ofid/ofz415.2491.

[57] K. Peng, L.K. Vora, J. Domínguez-Robles, Y.A. Naser, M. Li, E. Larrañeta, R. F. Donnelly, Hydrogel-forming microneedles for rapid and efficient skin deposition of controlled release tip-implants, Materials Sci. Eng.: C 127 (2021) 112226, https://doi.org/10.1016/j.msec.2021.112226.

[58] L.K. Vora, K. Moffatt, R.F. Donnelly, 9 - Long-lasting drug delivery systems based on microneedles. Long-Acting Drug Delivery Systems, Woodhead Publishing, 2022, pp. 249–287.